Deciphering the isotopic imprint of nitrate to reveal nitrogen source and transport mechanisms in a tile-drained agroecosystem

Yinchao Hu[1], Zhongjie Yu[1]*, Wendy H. Yang[2,3], Andrew J. Margenot[4], Lowell E. Gentry[1], Michelle M. Wander[1], Richard L. Mulvaney[1], Corey A. Mitchell[1], Carlos E. Guacho[1]

Departments of [1]Natural Resources and Environmental Sciences, [2]Plant Biology, [3]Earth Science and Environmental Change, and [4]Crop Sciences, University of Illinois at Urbana-Champaign, Urbana, Illinois, USA

*Corresponding author: zjyu@illinois.edu

Abstract

Installation of subsurface drainage systems has profoundly altered the nitrogen cycle in agricultural regions across the globe, facilitating substantial loss of nitrate (NO_3^-) to surface water systems. Lack of understanding of the sources and processes controlling NO_3^- loss from tile-drained agroecosystems hinders the development of management strategies aimed at reducing this loss. The natural abundance nitrogen and oxygen isotopes of NO_3^- provide a valuable tool for differentiating nitrogen sources and tracking the biogeochemical transformations acting on NO_3^-. This study combined multi-years of tile drainage measurements with NO_3^- isotopic analysis to examine NO_3^- source and transport mechanisms in a tile-drained corn-soybean field. The tile drainage NO_3^- isotope data were supplemented by characterization of the nitrogen isotopic composition of potential NO_3^- sources (fertilizer, soil nitrogen, and crop biomass) in the field and the oxygen isotopic composition of NO_3^- produced by nitrification in soil incubations. The results show that NO_3^- isotopes in tile drainage were highly responsive to tile discharge variation and fertilizer input. After accounting for isotopic fractionations during nitrification and denitrification, the isotopic signature of tile drainage NO_3^- was temporally stable and similar to those of fertilizer and soybean residue during unfertilized periods. This temporal invariance in NO_3^- isotopic signature indicates a nitrogen legacy effect, possibly resulting from N recycling at the soil microsite scale and a large water storage for NO_3^- mixing. Collectively, these

results demonstrate how combining field NO_3^- isotope data with knowledge of isotopic fractionations can reveal mechanisms controlling NO_3^- cycling and transport under complex field conditions.

Plain Language Summary

Installation of subsurface tile pipes in many poorly drained agricultural lands has facilitated a substantial loss of nitrate (NO_3^-) to surface water systems. However, the nitrogen sources and related processes controlling NO_3^- export from tile-drained agricultural systems remain unclear. This study employed stable isotope techniques to investigate how NO_3^- is biologically produced and hydrologically transported in a tile-drained field. Stable isotopes are chemical variants of the same element and have long been used as a tracer of nitrogen cycling in environmental systems. By combining field measurements of NO_3^- isotopes in tile drainage with a detailed understanding of how these isotopes are altered by microbial reactions, we estimated the original isotope ratios of NO_3^- and compared these ratios to those of potential nitrogen sources in the field. The results show that the original isotope ratios of NO_3^- were similar to those of ammonia fertilizer and soybean biomass nitrogen and did not vary over time when there was no fertilizer input to the system. These findings indicate the presence of a large NO_3^- pool in the soil and a time lag between the moments when the source nitrogen was introduced into the system and when the NO_3^- was exported via tile drainage.

Highlights

- The oxygen isotopic composition of nitrate produced by soil nitrification varied with the degree of soil nitrite accumulation.
- The dual isotopes of nitrate in tile drainage exhibited coupled variations and were highly responsive to variations in tile discharge.
- Combining field nitrate isotope data with the isotopic systematics of nitrification reveals a legacy effect controlling nitrate dynamics.

Keywords: tile drainage, nitrate isotopes, source partitioning, isotopic fractionation, nitrification, denitrification

1. Introduction

Chronic anthropogenic nitrogen (N) input into terrestrial and aquatic ecosystems exceeds established safe planetary boundaries, with detrimental consequences of biodiversity loss, water pollution, and deteriorating ecosystem resilience (Gruber and Galloway, 2008). In the U.S. Upper Midwest, approximately 40% of agricultural lands are currently drained by subsurface tiles to increase soil drainage for corn and soybean production (Castellano et al., 2019; Valayamkunnath et al., 2020). The installation of these drainage systems has profoundly altered regional hydrological and biogeochemical regimes, facilitating a substantial loss of nitrate (NO_3^-) via tile discharge (Blann et al., 2009). Indeed, the combination of N fertilizer applications on intensively tile-drained watersheds has been considered the dominant source of riverine NO_3^- yields in the Mississippi River Basin (David et al., 2010).

Despite well-documented environmental impacts, the sources and processes sustaining high NO_3^- export from tile-drained agricultural landscapes remain unclear. For example, while labeled ^{15}N tracer studies in the U.S. Corn Belt have consistently demonstrated that less than half of applied fertilizer N is recovered by the corn crop in the same year (Gardner and Drinkwater, 2009), it remains elusive how the majority of fertilizer N not recovered by the corn uptake is partitioned into various retention and loss pathways (Yan et al., 2020). Moreover, variations in NO_3^- load from many tile-drained fields and watersheds have been shown to scale linearly with precipitation and flow events (Bauwe et al., 2020; Danalatos et al., 2022), suggesting a biogeochemically stationary regime in NO_3^- export. This biogeochemical stationarity, often referred to as 'chemostasis' (Godsey et al., 2009), has been interpreted to indicate the presence of a large legacy N store resulting from NO_3^- accumulation in soil and groundwater systems and/or accretion and subsequent mineralization of soil organic N (Basu et al., 2010; Thompson et al., 2011; Van Meter et al., 2018). However, direct constraints and detailed mechanisms to corroborate this legacy N store in intensively managed agroecosystems are still lacking.

Enabled by methodological advances in the early 2000s, the last two decades have seen a bloom of studies that utilized the natural abundance $^{15}N/^{14}N$ and $^{18}O/^{16}O$ ratios of NO_3^- to investigate

reactive N in the environment. By convention, NO_3^- isotopes are reported using δ notation, where $\delta^{15}N=([^{15}N/^{14}N]_{sample}/[^{15}N/^{14}N]_{air}-1)\times1000$ and $\delta^{18}O=([^{18}O/^{16}O]_{sample}/[^{18}O/^{16}O]_{VSMOW}-1)\times1000$, in units of per mille (‰). As each isotope system offers complementary insights into NO_3^- sources and transformations (Fig. 1), dual analysis of $\delta^{15}N_{NO3}$ and $\delta^{18}O_{NO3}$ offers unique biogeochemical information unobtainable by bulk concentration measurement alone (Granger and Wankel, 2016). However, notwithstanding the increasing use of NO_3^- isotopes, there are persistent knowledge gaps in interpreting environmental NO_3^- isotope data for robust NO_3^- source characterization. For example, considerable uncertainties can result from simple mixing modeling of NO_3^- isotopes due to unknown or overlapping NO_3^- source endmembers (Kendall et al., 2007) (Fig. 1). Moreover, enzymatic bond breaking during microbial denitrification results in strong isotopic fractionation of NO_3^-, leading to substantial enrichment of heavier isotopes (^{15}N and ^{18}O) in the remaining NO_3^- (Mariotti et al., 1981). This denitrification isotope effect is expressed as a linear trajectory in the biplot of $\delta^{15}N_{NO3}$ and $\delta^{18}O_{NO3}$ (i.e., dual isotope space; Fig. 1), reflecting the coupling of N and O isotopic fractionations during the denitrification process (Granger et al., 2008; Boettger et al., 2022). While the expression of these isotopic fractionations can be a valuable tool for quantifying the occurrence and intensity of denitrification, the large isotopic enrichment resulting from denitrification obscures the original isotopic signature of NO_3^- and, therefore, requires careful corrections for N source partitioning using NO_3^- isotopes.

At the other end of the biogeochemical NO_3^- cycle, nitrification determines the initial isotopic imprint of NO_3^- produced from organic and ammoniacal N, which comprise the major anthropogenic and soil sources of NO_3^- in agricultural landscapes (Fig. 1). Previous studies of pure cultures and soil incubations have demonstrated a significant kinetic N isotope effect for the two-step nitrification of NO_3^- from ammonia (NH_3) (Casciotti et al., 2003; Yu and Elliott, 2018). Consequently, when NH_3 supply is high, such as after fertilizer applications, the $\delta^{15}N_{NO3}$ produced from nitrification is much lower than the $\delta^{15}N$ of the source NH_3. For the $\delta^{18}O_{NO3}$ produced from nitrification (denoted as $\delta^{18}O_{NO3,nit}$), it is commonly assumed that, for the three O atoms of NO_3^- produced from bacterial nitrification, two O atoms are derived from water and one from O_2 (Andersson and Hooper, 1983;

Kumar et al., 1983). Accordingly, $\delta^{18}O_{NO3,nit}$ has been construed to vary over the range of -10 to 10‰ (Fig. 1) (Kendall et al., 2007) given the $\delta^{18}O$ of atmospheric O_2 (23.5‰) (Kroopnick and Craig, 1972) and the normal $\delta^{18}O$ range of environmental water (-25 to 4‰). However, recent studies of bacterial and archaeal pure cultures and freshwater assemblages have revealed a complex isotopic systematics of $\delta^{18}O_{NO3,nit}$ that includes kinetic fractionation during the incorporation of O atoms from water and O_2 into the NO_3^- produced, as well as equilibrium fractionation occurring during the exchange of O atoms between water and nitrite (NO_2^-), which is an intermediate of nitrification (Casciotti et al., 2010; Buchwald and Casciotti, 2010; Nishizawa et al., 2016; Boshers et al., 2019) (Inset in Fig. 1). Importantly, a robust predictive understanding of $\delta^{18}O_{NO3,nit}$ is vital to pinpointing the origin of the denitrification line in dual isotope space, where the corresponding value on the $\delta^{15}N_{NO3}$ axis represents the source signature of the nitrified NO_3^-, corrected for denitrification enrichment (Fig. 1). Despite its necessity for unbiased NO_3^- source partitioning, only one study (Snider et al., 2010) has thus far quantified O isotopic fractionations and exchange during soil nitrification. It remains unresolved whether isotopic systematics of $\delta^{18}O_{NO3,nit}$ based on pure cultures can be generalized to nitrification catalyzed by complex soil nitrifying communities and how changes in soil state variables (e.g., substrate availability) may influence the variability of $\delta^{18}O_{NO3,nit}$.

This study presents results from a comprehensive investigation of NO_3^- isotopes in a tile-drained field under a corn-soybean rotation, representative of the U.S. Corn Belt. Given the potential for NO_3^- isotopes to summarize NO_3^- source and transformation mechanisms, we expected combining long-term tile drainage measurements with NO_3^- isotopic analysis to provide new insights into the sources and processes controlling tile drainage NO_3^- export. A unique aspect of this work is that the N isotopic composition of potential sources of NO_3^- in tile drainage, including fertilizer, soil N, and crop residues, were directly measured. Additionally, laboratory soil incubations were conducted to quantify isotope effects controlling $\delta^{18}O_{NO3,nit}$ under different nitrification conditions. These characterized source endmembers and isotope effects were then combined with NO_3^- isotopes measured in tile drainage to tease apart potentially intertwined mechanisms for NO_3^- transport and source variations. To our knowledge, this work represents the first attempt to employ such a fine-grained approach to

tackle NO_3^- sources and transport in terrestrial settings. We postulated that if tile drainage NO_3^- loss was directly controlled by management and biogeochemical processes, such as fertilizer input, crop rotation, and mineralization of soil organic N, the isotopic signature of NO_3^- after accounting for isotopic fractionations during nitrification and denitrification would reflect the dynamic source contributions. Additionally, the isotopic signature of NO_3^- would be temporally stable if NO_3^- in tile drainage was dominantly sourced from a large and well-mixed legacy N store in the soil-plant system.

2. Materials and Methods

2.1. Site description and tile drainage management.

The study field is located within the Upper Embarras River watershed near Tuscola, Illinois (39°43′ N, 88°14′ W). This site is representative of the recently glaciated Midwest, characterized by low-gradient topography and poorly drained soils classified as fine, mixed, superactive, mesic Typic Endoaquolls (Milford series) (USDA-NRCS, 2016). The system of parallel drains at this field was installed approximately 40 years ago at depths ranging from 1.2 to 1.5 m below the soil surface, and is composed of one main drain fed by a set of lateral drains spaced 30.5 m apart, all consisting of 12.7 cm diameter perforated plastic pipe (Fig. S1). Starting in 2015, each lateral tile was monitored for a replicated fertilizer management study using inline water level control structures (AgriDrain Corporation, USA) (Gentry et al., 2023).

The current study focuses on field-scale observations of three lateral tiles, hereafter referred to as Tiles A, B, and C (Fig. S1). Each study tile is 500 to 570 m in length and drains an area of approximately 1.7 ha. Identical agricultural management practices were applied to the soil overlying the three tiles. Briefly, a two-year crop rotation of corn-soybean, the dominant cropping scheme in the Upper Midwest, was used. During the period of this study (October 2020 to August 2023), corn was planted in 2021 and 2023, and soybean in 2022. One to 14 days prior to corn planting, anhydrous NH_3 was knifed into the surface soil at a rate of 200 kg N ha^{-1}. No N fertilizer was applied to soybean. It is noteworthy that no NO_3^- fertilizer was applied to the study tiles between 2015 and 2023. This allows us to examine the extent to which a better accounting of nitrification and denitrification isotope effects can improve the isotopic fingerprinting of NO_3^-, without being affected by confounding effects

resulting from external NO_3^- input. Likewise, atmospheric NO_3^- deposition, which was approximately 5 kg N ha^{-1} during the study period (NADP, 2023), is deemed negligible compared to annual N input via fertilizer application and crop residue incorporation (> 400 kg N ha^{-1}). While soybean was no-till planted, the seedbed for corn was prepared by strip-tillage. As is typical in the region, the field is rainfed and not irrigated, so the only water input was precipitation.

Throughout the study period, tile discharge at each tile was measured using the inline control structure and a pressure transducer (see Yu et al. (2023) for more details). We collected weekly water samples from each of the three control structures when the tiles were flowing (n = 351). These samples were vacuum filtered and frozen until concentration and isotopic (NO_3^- and water) analyses. Additionally, from April 2022 to August 2023, a custom-made bulk precipitation collector was deployed at the site to collect weekly cumulative precipitation samples for water isotope analysis.

2.2. Quantification of tile NO_3^- load and NO_3^- export regime.

Daily NO_3^- loads in tile drainage were linearly extrapolated to estimate annual loads based on water year, defined as October 1 to September 31. The export regime of NO_3^- in tile drainage was quantified using the method of Godsey et al. (2009). For this analysis, measured NO_3^- concentrations and corresponding tile discharge were log-transformed, and the linear slope of the log-log regression of discharge and concentration was used to categorize NO_3^- export regime into chemostatic (slope ≈ 0) and non-chemostatic (slope significantly different than zero) patterns. To examine the effects of crop rotation and fertilizer input on NO_3^- export regime, we classified NO_3^- and tile discharge data by crop year (i.e., water year with corn or soybean being cultivated), and further divided the corn data into growing season and non-growing season based on the timing of spring N fertilizer application. Therefore, the corn non-growing season spans from the dormant period of a corn year until spring fertilizer application, followed by the corn growing season, which starts at fertilizer application and ends at corn harvest. This distinction of cropping phases is operationally defined and aligns well with the onset and cessation of tile drainage in the field (see below).

2.3. Determination of NO_3^- source endmembers.

We collected numerous surface soil samples (0-20 cm) from two locations at each study tile immediately following the application of anhydrous NH_3 fertilizer in April 2021, targeting the area where NH_3 was knife-injected. The collected samples were combined into six composite samples for determination of the $\delta^{15}N$ of soil ammonium (NH_4^+), which was used to represent the $\delta^{15}N$ of applied NH_3 fertilizer. Near the end of the growing seasons of 2021 and 2022 (i.e., at the R6 growth stage), we collected aboveground corn and soybean biomass for N isotopic analysis. Two 5 by 5 m microplots were established overlying each tile, offset from the center, for collection of eight corn plants in 2021 and 15 soybean plants in 2022 from each microplot. Biomass samples collected from each microplot were first separated into grain and stover and then respectively combined to generate composite samples. Additionally, we collected one soil core to a depth of 90 cm within each microplot following the crop biomass sampling in 2021 and 2022. These soil cores were sectioned at 0-15, 15-30, 30-60, and 60-90 cm depths for isotopic analyses of soil total N (TN).

2.4. Laboratory nitrification experiment.

Following soybean harvest in 2022, we sampled surface soil (0-30 cm) from two locations at each tile and combined all collected samples to generate a composite sample for a laboratory nitrification experiment. The physical and chemical properties of this composite soil are provided in Table S1. We slurred the soil for this experiment to provide a homogenized environment for characterizing integrated isotopic fractionations catalyzed by the soil microbial community (Taylor et al., 2019). The experimental protocol largely followed those developed for quantifying $\delta^{18}O_{NO3,nit}$ using nitrifier pure cultures (Casciotti et al., 2010; Buchwald and Casciotti, 2010). Specifically, we established two NH_4^+ fertilization treatments, 100 mg N kg dry $soil^{-1}$ and 0 mg N kg dry $soil^{-1}$, to quantify how $\delta^{18}O_{NO3,nit}$ values change with soil nitrification rate. The fertilized treatment was designed to mimic high soil NH_4^+ conditions following field fertilizer applications (i.e., the initial concentration of 100 mg N kg dry $soil^{-1}$ is roughly equivalent to an application rate of 224 kg N ha^{-1}).

For each fertilization treatment, we established three parallel $\delta^{18}O_{H2O}$ treatments, -6.8‰, 21.3‰, and 49.1‰, each with three replicates, to quantify O isotope exchange and fractionations during nitrification. These parallel treatments were established by mixing laboratory de-ionized water

and ^{18}O-labeled water (10% atom percent; Cambridge Isotope Laboratory). To set up the incubation, replicate samples (n=72 for the fertilized treatment and n=63 for the non-fertilized treatment) were prepared by combining 8 grams of soil (dry weight equivalent) with 10 mL of de-ionized water in a 50-mL centrifuge tube and then preincubated for 24 h. To initiate the incubation, 30 mL of water containing different amounts of ^{18}O-labeled water and a $(NH_4)_2SO_4$ solution was added to each tube to achieve a 1:5 soil-to-water ratio and the desired NH_4^+ fertilization and $\delta^{18}O_{H2O}$ levels. The soil slurries were then incubated at room temperature (21 °C) on a horizontal shaker and sampled at intervals of 0.5 to 14 h over a 72-h period. For each incubation interval, a set of replicate slurry were sampled by centrifuging at 2000 rpm for 10 min, and the supernatants were filtered through a sterile 0.2 μm filter. We briefly opened the caps of remaining slurry samples every 24 h to ensure aerobic incubation conditions. We note that the ^{18}O-labeled water contained a trace amount of background NO_3^- (~0.1 μg N L^{-1}). Preliminary measurements showed that this background NO_3^- to be at natural abundance with respect to ^{18}O (~20‰) and thus had a negligible impact on the determination of $\delta^{18}O_{NO3,nit}$; however, the ^{15}N enrichment exceeded 10% atom percent. Therefore, $\delta^{15}N_{NO3}$ results are only reported when there was no addition of ^{18}O-labeled water (i.e., for the treatment with $\delta^{18}O_{H2O}$ = -6.8‰).

2.5. Quantification of $\delta^{18}O_{NO3,nit}$ and underlying isotopic fractionations and exchange

For both the fertilized and non-fertilized treatments of the nitrification experiment, we calculated $\delta^{18}O_{NO3,nit}$ using NO_3^- concentrations and $\delta^{18}O_{NO3}$ values measured at the beginning and end of the incubation. Therefore, these $\delta^{18}O_{NO3,nit}$ values represent the $\delta^{18}O$ of net NO_3^- produced during the entire incubation period. To elucidate the fractionation mechanisms underlying $\delta^{18}O_{NO3,nit}$, we adopted the established isotope model of bacterial and archaeal nitrification that considers kinetic and equilibrium O isotope effects for the two-step production of NO_3^- from NH_3 via NO_2^- (Casciotti et al., 2010; Buchwald and Casciotti, 2010) (Fig. 1 insert):

$$\delta^{18}O_{NO3,nit} = \frac{2}{3}\left\{(1-f_{ex})\left[\frac{1}{2}\left(\delta^{18}O_{O2} + {}^{18}\varepsilon_{k,O2}\right) + \frac{1}{2}\left(\delta^{18}O_{H2O} + {}^{18}\varepsilon_{k,H2O,1}\right)\right] + f_{ex}\left(\delta^{18}O_{H2O} + {}^{18}\varepsilon_{eq}\right)\right\} + \frac{1}{3}\left(\delta^{18}O_{H2O} + {}^{18}\varepsilon_{k,H2O,2}\right) \quad \text{(Eq. 1)}$$

In Eq. 1, $\delta^{18}O_{O2}$ is the $\delta^{18}O$ of O_2, $^{18}\varepsilon_{k,O2}$ is the kinetic isotope effect for O_2 incorporation, $^{18}\varepsilon_{k,H2O,1}$ is the kinetic isotope effect for water incorporation during NH_3 oxidation to NO_2^-, $^{18}\varepsilon_{k,H2O,2}$ is the kinetic isotope effect for water incorporation during NO_2^- oxidation to NO_3^-, f_{ex} is the fraction of O atoms in NO_2^- that have exchanged with water, and $^{18}\varepsilon_{eq}$ is the equilibrium isotope fractionation factor for NO_2^- isotopic exchange. The O isotope effect associated with NO_2^- oxidation to NO_3^- ($^{18}\varepsilon_{k,NO2}$; Fig. 1 insert) is not included in Eq. 1 because this isotope effect was not expressed due to the near complete NO_2^- oxidation by the end of the incubation (see below). Eq. 1 can be rearranged to conform to a linear formulation of $\delta^{18}O_{NO3,nit}$ versus $\delta^{18}O_{H2O}$:

$$\delta^{18}O_{NO3,nit} = \left(\frac{2}{3} + \frac{1}{3}f_{ex}\right)\delta^{18}O_{H2O} + \frac{1}{3}\left[\left(\delta^{18}O_{O2} - {}^{18}\varepsilon_{k,O2} - {}^{18}\varepsilon_{k,H2O,1}\right)(1 - f_{ex}) - {}^{18}\varepsilon_{k,H2O,2}\right] + \frac{2}{3}\left(f_{ex}\,{}^{18}\varepsilon_{eq}\right) \quad \text{(Eq. 2)}$$

From Eq. 2, f_{ex} can be estimated using the slope of a linear regression of $\delta^{18}O_{NO3,nit}$ versus $\delta^{18}O_{H2O}$ across the three parallel $\delta^{18}O_{H2O}$ treatments. The intercept expression shown in Eq. 2 is a function of f_{ex}, $\delta^{18}O_{O2}$, and four O isotope effects ($^{18}\varepsilon_{k,O2}$, $^{18}\varepsilon_{k,H2O,1}$, $^{18}\varepsilon_{k,H2O,2}$, and $^{18}\varepsilon_{eq}$). We combined $^{18}\varepsilon_{k,O2}$ and $^{18}\varepsilon_{k,H2O,1}$ into a composite O isotope effect ($^{18}\varepsilon_{comp}$) to represent the lumped $\delta^{18}O$ offset between NO_2^- produced from NH_3 and its O substrates (O_2 and water) (Casciotti et al., 2010). Furthermore, we assumed that $^{18}\varepsilon_{comp}$ and $^{18}\varepsilon_{k,H2O,2}$ were constant between the fertilized and non-fertilized treatments. This allows us to solve for $^{18}\varepsilon_{comp}$ and $^{18}\varepsilon_{k,H2O,2}$ using regression intercepts derived from the fertilized and non-fertilized incubations by further assuming a $\delta^{18}O_{O2}$ value of 23.5‰ and a $^{18}\varepsilon_{eq}$ value of 13‰ for both abiotic and enzyme-catalyzed O exchange (Casciotti et al., 2007; Buchwald and Casciotti, 2013) (i.e., solving two unknowns using a system of two equations).

2.6. NO_3^- source characterization.

We estimated the source signature of tile drainage NO_3^- under in situ conditions (denoted as $\delta^{15}N_{source}$) by combining measured tile drainage NO_3^- isotopes with the O isotopic systematics of NO_3^- quantified in the soil nitrification experiment. Specifically, we applied measured tile drainage $\delta^{18}O_{H2O}$ in the empirical relationships of $\delta^{18}O_{NO3,nit}$ versus $\delta^{18}O_{H2O}$ derived from the nitrification experiment to predict $\delta^{18}O_{NO3,nit}$ under in situ conditions. These predicted $\delta^{18}O_{NO3,nit}$ values were then compared to

measured $\delta^{18}O_{NO3}$ values in tile drainage to estimate the isotopic enrichment of NO_3^- resulting from denitrification. Subsequently, we derived $\delta^{15}N_{source}$ by subtracting the estimated denitrification enrichment from measured $\delta^{15}N_{NO3}$ values. Graphically, this approach is essentially a linear projection in dual isotope space, where a measured data point is mapped to the predicted $\delta^{18}O_{NO3,nit}$ by following a denitrification trajectory with a slope of one. $\delta^{15}N_{source}$ is then obtained as the corresponding value on the $\delta^{15}N_{NO3}$ axis (Fig. 1). Importantly, this method for estimating $\delta^{15}N_{source}$ is dependent upon two critical assumptions: (1) the $\delta^{18}O$ of water used by the soil nitrifiers is equal to that measured for tile drainage, and (2) denitrification fractionates NO_3^- isotopes along a linear trajectory with a slope of one in dual isotope space. These assumptions will be addressed before any conclusions are reached.

2.7. Chemical and isotopic analyses.

Tile drainage and soil incubation samples were analyzed for NO_3^- and NO_2^- concentrations using a Dionex ICS1600 Ion Chromatograph. The $\delta^{15}N$ and $\delta^{18}O$ of NO_3^- were measured after conversion to N_2O by the denitrifier method (Weigand et al., 2016), using an Elementar Isoprime isotope ratio mass spectrometer (IRMS). Prior to NO_3^- isotopic analysis, any detectable NO_2^- was removed by decomposition using sulfamic acid (Granger and Sigman, 2009). International NO_3^- reference materials USGS34 and USGS35 and an internal NO_3^- working standard were used to calibrate $\delta^{15}N_{NO3}$ and $\delta^{18}O_{NO3}$ analyses, for which the precision was ±0.1‰ in the former case and ±0.3‰ in the latter. We measured the O and H isotopes of tile drainage water and on-site precipitation using wavelength-scanned cavity ring-down spectroscopy on a Picarro Model L2130-i. The spectroscopic measurements were made against laboratory reference materials calibrated to VSMOW, with a precision of ±0.1‰ for $\delta^{18}O_{H2O}$ and ±0.5‰ for $\delta^{2}H$. Ammonium and NO_3^- in the soil samples collected following anhydrous NH_3 application were extracted using 2 M KCl and measured using a SmartChem 200 discrete flow analyzer. The $\delta^{15}N$ value of extracted NH_4^+ was determined by coupling the persulfate oxidation and the denitrifer method (Yu and Elliott, 2018). The collected soil core samples and crop biomass were oven-dried (60 °C) for 6 days and finely ground for $\delta^{15}N$ analysis using an elemental analyzer coupled with an IRMS.

2.8. Statistical analysis.

Ordinary linear regression was used to examine the relationships between $\delta^{15}N_{NO3}$ and $\delta^{18}O_{NO3}$ in tile drainage and between $\delta^{18}O_{H2O}$ and $\delta^{18}O_{NO3,nit}$ measured in the nitrification experiment. We used analysis of covariance (ANCOVA) followed by Fisher's least significant difference procedure to detect significant differences in linear regression slope among groups. All statistical analyses were conducted using MATLAB and were evaluated at a significance level of 0.05.

3. Results

3.1. Soil nitrification experiment.

Following NH_4^+ fertilization, NO_3^- concentrations increased slowly over the first 36 hours of the incubation, followed by a much more rapid increase to peak concentrations of 94.2–99.1 mg N kg dry soil^{-1} at 72 hours (Fig. 2a). The amounts of NO_3^- produced during the incubations were greater than 90% of the amended NH_4^+ (i.e., 100 mg N kg dry soil^{-1}) for all replicates, equivalent to a net NO_3^- production rate of approximately 32 mg N kg dry soil^{-1} d^{-1}. NO_2^- was detectable at the beginning of the incubation, reached maximum concentrations of 7.2–7.7 mg N kg dry soil^{-1} between hours 48 and 58, and then decreased to less than 2 mg N kg dry soil^{-1} at the end of the incubation. At that time, NO_2^- constituted less than 3% of the total $NO_3^- + NO_2^-$ pool (Fig. 2a). $\delta^{15}N_{NO3}$ values decreased sharply to -22.1‰ following the onset of NO_3^- production, reaching a minimum of -24.2‰ at 14 hours (Fig. 2b). As NO_3^- production proceeded, $\delta^{15}N_{NO3}$ values gradually increased and eventually approached the initial $\delta^{15}N$ of the amended NH_4^+ (i.e., 0.1‰). This temporal progression of $\delta^{15}N_{NO3}$ can be well explained by a kinetic N isotope effect for NH_4^+ oxidation, which was estimated to be 25.3‰ by fitting a closed-system Rayleigh product equation (Fig. S3).

Compared to the fertilized treatment, the net rates of NO_3^- production were much lower under the non-fertilized treatment (Fig. 2d), and the amount of NO_3^- produced over the entire incubation ranged between 4.3 and 5.8 mg N kg dry soil^{-1}. During the net NO_3^- production, $\delta^{15}N_{NO3}$ values increased from 4.8‰ to 7.2‰ by hour 12 and then gradually decreased to 3.2‰ at the end of the incubation (Fig. 2e). This steady decline in $\delta^{15}N_{NO3}$ observed after hour 12 corresponds to a $\delta^{15}N$ value of net produced NO_3^- of -0.8‰. NO_2^- was not detectable throughout the non-fertilized incubation.

The temporal progression of $\delta^{18}O_{NO3}$ values was similar in the fertilized and non-fertilized treatments (Fig. 2c and 2f). Specifically, $\delta^{18}O_{NO3}$ values varied among the three $\delta^{18}O_{H2O}$ treatments at the onset of NO_3^- production, reflecting mixing of newly produced NO_3^- with the background pool of soil NO_3^-. With fertilization, $\delta^{18}O_{NO3}$ values evolved gradually, obtaining final values of -2.2 to 45.2‰ for the three $\delta^{18}O_{H2O}$ treatments. In comparison to the fertilized treatment, the final $\delta^{18}O_{NO3}$ values without fertilization varied over a narrower range of -3.4 to 28.8‰. The estimated $\delta^{18}O_{NO3,nit}$ values correlated linearly with $\delta^{18}O_{H2O}$ across the three parallel $\delta^{18}O_{H2O}$ treatments (Fig. 3), giving a slope (±1 SE) of 0.86±0.00 and an intercept (±1 SE) of 3.56±0.05 for the fertilized treatment, while the corresponding values for the non-fertilized treatment were 0.67±0.01 and -1.62±0.21. Based on Eq. 2 and the estimated regression slopes, f_{ex} was estimated to be 59±0% and 0±3% for the fertilized and non-fertilized treatments, respectively. For both fertilized and non-fertilized treatments, $^{18}\varepsilon_{comp}$ and $^{18}\varepsilon_{k,H2O,2}$ were estimated using the regression intercepts to be 24.3±1.0‰ and 4.5±0.4‰, respectively.

3.2. Tile discharge and NO_3^- concentrations.

The quantity and duration of tile discharge in the field varied interannually during the study period (Fig. 4). Each water year, tile flow ceased in the early peak growing season (i.e., late July to early August) due to enhanced crop evapotranspiration. The onset of tile discharge was more variable and largely dependent on triggering precipitation events following crop harvest. On average across all three tiles, the total tile discharge (±1 SD) was 303±14 mm, 324±13 mm, and 217±14 mm for the three years, respectively. The annual NO_3^- loads (±1 SD) were higher in the 2021 corn year and the 2022 soybean year (25.8±3.7 and 26.3±3.4 kg N ha^{-1}, respectively) than in the 2023 corn year (21.1±2.6 kg N ha^{-1}).

Tile NO_3^- concentrations were more variable during the two corn years (2021 and 2023), as compared to the 2022 soybean year (Fig. 4b). Specifically, while NO_3^- concentrations increased at a slow rate during the corn non-growing season in 2021 and 2023, dramatic increases in NO_3^- concentrations were observed in tile drainage following fertilizer input. This was particularly the case following fertilizer application in 2021, where consecutive precipitation events triggered extended tile flows and a substantial loss of NO_3^- in tile drainage. Among the three tiles, Tile A had consistently

lower NO_3^- concentrations, possibly due to fine-scale soil property variation as this tile intersects more depression areas than the other two tiles (Fig. S1). For all three cropping phases (i.e., corn growing season, corn non-growing season, and soybean year) and three individual tiles, the log-log slope of NO_3^- concentration versus tile discharge was essentially zero (i.e., absolute magnitude less than 0.04), and none of the log-log regression fits was statistically significant (Fig. 5 left column). These results indicate a persistent chemostasis in tile NO_3^- export.

3.3. Variations in NO_3^- isotopes in tile drainage.

NO_3^- isotopes in tile drainage varied distinctly with the cropping phases (Fig. 4c and 4d). Both $\delta^{15}N_{NO3}$ and $\delta^{18}O_{NO3}$ values declined steadily by 4-5‰ during the corn non-growing season in 2021 and 2023. Following fertilizer application and at the initiation of the corn growing season in 2021, $\delta^{15}N_{NO3}$ values declined shapely to as low as -5‰. However, this period of low $\delta^{15}N_{NO3}$ was short-lived, as $\delta^{15}N_{NO3}$ values increased rapidly with declining tile discharge toward the peak growing season. As documented by Fig. 4c, a similar response of $\delta^{15}N_{NO3}$ was also observed following fertilizer application in 2023, albeit to a lesser extent due to drier conditions in the early summer of 2023 (Fig. 4a). Compared to $\delta^{15}N_{NO3}$ values, $\delta^{18}O_{NO3}$ values exhibited a steeper increase during the corn growing season, and a strong response to fertilizer input was generally lacking (Fig. 4d). Tile drainage $\delta^{15}N_{NO3}$ and $\delta^{18}O_{NO3}$ values measured during the soybean year varied over relatively narrower ranges and were generally similar to those measured at the end of the 2021 corn year.

In contrast to tile drainage NO_3^- concentration, both $\delta^{15}N_{NO3}$ and $\delta^{18}O_{NO3}$ values were highly responsive to tile discharge variation. This was especially the case during the corn non-growing season, when lower $\delta^{15}N_{NO3}$ and $\delta^{18}O_{NO3}$ values were consistently observed during high flow events (i.e., tile discharge > 1 mm d^{-1}; Fig. 5). This high sensitivity to flow event was confirmed by a significant and negative linear relationship between the two isotopes and the logarithm of tile discharge across three cropping phases and monitored tiles (Fig. 5 middle and right columns).

Plotting the measured $\delta^{15}N_{NO3}$ and $\delta^{18}O_{NO3}$ values revealed significant yet variable linear relationships in dual isotope space (Fig. 6). Specifically, $\delta^{15}N_{NO3}$ and $\delta^{18}O_{NO3}$ values measured during the corn non-growing season and soybean year appeared to follow a similar linear trajectory, while

those measured during the corn growing season were more scattered due to low $\delta^{15}N_{NO3}$ values observed following fertilizer applications. Results from an ANCOVA confirmed that the slope of the $\delta^{15}N_{NO3}$-versus-$\delta^{18}O_{NO3}$ relationship was not significantly different between the corn non-growing season and soybean year for Tiles B and C but was higher in either of these two phases without N fertilizer than in the corn growing season (Table S2). For Tile A, the slope was not significantly different among the three cropping phases (Table S2). Therefore, for consistency across the three tiles, we fit two regression lines to NO_3^- isotopes measured from each tile to best characterize the linear coupling of $\delta^{15}N_{NO3}$ and $\delta^{18}O_{NO3}$ values – one regression for all measurements and one regression for measurements during the corn non-growing season and soybean year only. The slopes of the regression lines based on the corn non-growing season and soybean year ranged from 0.90 to 1.06 across the three tiles (Fig. 6; Table S2). Including isotope data measured during the corn growing season significantly lowered the estimated slopes from near one to a range of 0.58 to 0.64 for the three tiles (Fig. 6; Table S2).

3.4. Water isotopes in tile drainage.

The $\delta^{18}O_{H2O}$ values of tile discharge varied between -7.4‰ and -5.5‰ throughout the study period (Fig. 4e). Variations in the $\delta^{18}O_{H2O}$ of tile discharge were highly dampened with respect to the $\delta^{18}O_{H2O}$ of precipitation, which varied between -16.6‰ and 0.7‰. Nevertheless, some synchronicities between the $\delta^{18}O_{H2O}$ values of precipitation and tile discharge were evident in the period for which contemporaneous tile discharge and precipitation measurements were available. Moreover, during individual flow events, the $\delta^{18}O_{H2O}$ of tile discharge can often be characterized by transient fluctuations that were correlated with the $\delta^{18}O_{H2O}$ of precipitation (Fig. 4e). Plotting the $\delta^{18}O_{H2O}$ and $\delta^{2}H$ values of tile drainage revealed a close alignment with the local meteoric water line based on the precipitation isotopes (Fig. S2), indicating that water isotopes in tile drainage were unaffected by evaporative enrichment.

3.5. NO_3^- source endmembers.

The $\delta^{15}N$ value (±1 SD) of soil NH_4^+ collected following anhydrous NH_3 application was -0.6±1.9‰ (Fig. 7). The $\delta^{15}N$ values of soil TN did not differ between the two sampling years, and the average

values for the four soil layers varied over a narrow range of 5.1 to 5.5‰. Based on all soil core samples collected, the concentration-weighted average $\delta^{15}N$ value of soil TN was 5.3±0.7‰. Using $\delta^{15}N$ values determined for corn grain (5.3±0.3‰) and stover (7.4±0.7‰), a weighted sum of 5.8±0.3‰ was obtained for total corn aboveground biomass N. The $\delta^{15}N$ values of soybean grain (-0.2±0.1‰) and stover (-0.3±0.4‰) were indistinguishable, and the $\delta^{15}N$ value of total soybean biomass N was estimated to be -0.2±0.1‰ (Fig. 7).

3.6. NO_3^- source characterization.

Given the distinct responses of NO_3^- isotopes to different cropping phases (Fig. 4), we calculated NO_3^- load-weighted mean values of $\delta^{15}N_{NO3}$ and $\delta^{18}O_{NO3}$ for each cropping phase to estimate $\delta^{15}N_{source}$. Across all three cropping phases and three tiles, these values ranged from 1.9‰ to 11.2‰ for $\delta^{15}N_{NO3}$ and from 3.2‰ to 8.0‰ for $\delta^{18}O_{NO3}$ (Fig. 7). To account for the effect of variable nitrification rate on $\delta^{18}O_{NO3,nit}$ and thusly on $\delta^{15}N_{source}$, we predicted $\delta^{18}O_{NO3,nit}$ as a range of values using the two $\delta^{18}O_{NO3,nit}$-versus-$\delta^{18}O_{H2O}$ relationships derived from the fertilized and non-fertilized soil incubations (Fig. 3). For illustrative purposes, in Fig. 7, we show source characterization results using the NO_3^- load-weighted mean $\delta^{18}O_{H2O}$ value of tile drainage for all three tiles (i.e., -6.3‰). In this case, $\delta^{18}O_{NO3,nit}$ was predicted to range between -5.8‰ and -1.9‰ using the two derived $\delta^{18}O_{NO3,nit}$-versus-$\delta^{18}O_{H2O}$ relationships (horizontal lines in Fig. 7). Based on this range of $\delta^{18}O_{NO3,nit}$, $\delta^{15}N_{source}$ values were estimated to vary between -8.4‰ and 1.3‰ when combining all three tiles and cropping phases (grey shaded area in Fig. 7).

Source characterization results based on $\delta^{18}O_{H2O}$ values specific to each tile and cropping phase are shown in Table 1. When considering all three tiles collectively, $\delta^{15}N_{source}$ values were estimated to vary over a range of -8.3‰ to -3.0‰ for the corn growing season, -4.4‰ to 0.8‰ for the corn non-growing season, and -4.8 to 1.4‰ for the soybean year (Table 1). Notably, $\delta^{15}N_{source}$ values were not significantly different between the corn non-growing season and soybean year as indicated by the overlapping ranges, whereas $\delta^{15}N_{source}$ values estimated for the corn growing season were generally lower.

4. Discussion

4.1. Oxygen isotope systematics of NO_3^- produced by soil nitrification

The results from the nitrification experiment, which revealed a linear dependence of $\delta^{18}O_{NO3,nit}$ on $\delta^{18}O_{H2O}$, are consistent with previous pure culture studies (Casciotti et al., 2010; Buchwald and Casciotti, 2010). It appears that this dependence on $\delta^{18}O_{H2O}$ varied with NH_4^+ availability and nitrification rate, as indicated by the significantly different slope and intercept of the $\delta^{18}O_{NO3,nit}$-versus-$\delta^{18}O_{H2O}$ relationship between the fertilized and non-fertilized treatments (Fig. 3). The range of f_{ex} (0-59%) derived based on a single soil in this study falls within the range reported by Snider et al. (2010) for three different agricultural and forest soils (37-88%) but is wider than those observed in NH_3 and NO_2^- oxidizing cultures grown under conditions relevant to marine nitrification (0-30%) (Casciotti et al., 2010; Buchwald et al., 2012).

The observed variability of $\delta^{18}O_{NO3,nit}$ and f_{ex} and their dependence on NH_4^+ availability and nitrification rates can be explained by the accumulation of NO_2^- as a nitrification intermediate. Specifically, high NH_4^+ availability in the fertilized treatment would be expected to stimulate the growth of NH_3 oxidizing bacteria/archaea, resulting in increased intra- and extracellular NO_2^- concentrations and acidic pH in the cellular periplasm (Andersson et al., 1982). This combination of high NO_2^- abundance and low pH may accelerate both abiotic exchange between NO_2^- and water and biologically mediated exchange occurring during NH_3 oxidation (Casciotti et al., 2007; Boshers et al., 2019). Consequently, the substantial exchange between NO_2^- and water under the fertilized condition resulted in a higher sensitivity of $\delta^{18}O_{NO3,nit}$ to variations in $\delta^{18}O_{H2O}$, as reflected by the higher slope for the $\delta^{18}O_{NO3,nit}$-versus-$\delta^{18}O_{H2O}$ relationship (Fig. 3). Moreover, the equilibrium isotope effect for NO_2^- isotopic exchange (as represented by $^{18}\varepsilon_{eq}$) dictates that at equilibrium, the $\delta^{18}O$ of NO_2^- is higher than $\delta^{18}O_{H2O}$ by 13‰. The propagation of the impact of this equilibrium fractionation into the NO_3^- produced can explain why final $\delta^{18}O_{NO3}$ values were higher for the fertilized than non-fertilized incubation, which likewise led to a larger intercept of the $\delta^{18}O_{NO3,nit}$-versus-$\delta^{18}O_{H2O}$ relationship (Fig. 3). On the other hand, nitrification in the absence of ammoniacal fertilization was limited by NH_3 production from soil organic N (ammonification). This substrate limitation facilitated a tighter coupling of NH_3 and NO_2^- oxidation and consequently prevented NO_2^- accumulation and NO_2^-

454 isotopic exchange. Importantly, NO_2^- accumulation is frequently reported for agricultural soils after N
455 fertilizer applications (Jones and Hedlin, 1970; Smith et al., 1997; Venterea, 2007; Maharjan and
456 Venterea, 2013). This accumulation can be attributed to a delay in protein synthesis by NO_2^- oxidizing
457 bacteria in response to increased NH_3 oxidation rates (Giguere et al., 2018) or to a kinetic constraint
458 that requires moderate NO_2^- accumulation to balance the rates of NH_3 and NO_2^- oxidation (Taylor et
459 al., 2019). Therefore, it can be assumed that the variable f_{ex} and $\delta^{18}O_{NO3,nit}$ observed in our soil
460 incubations are representative of those mediated by nitrifier communities in agricultural soil, where
461 large variation in substate availability is common following fertilizer application.

462 Our estimate of $^{18}\varepsilon_{comp}$ (24.3±1.0‰) is well within the range previously reported for NH_3-
463 oxidizing bacteria and archaea (18-38‰) (Casciotti et al., 2010; Nishizawa et al., 2016), whereas the
464 estimated $^{18}\varepsilon_{k,H2O,2}$ (4.5±0.4‰) is lower than the reported range for NO_2^--oxidizing bacteria (9-25‰)
465 (Buchwald and Casciotti, 2010). We are unable to resolve whether the lower $^{18}\varepsilon_{k,H2O,2}$ from our soil
466 incubations is due to an intrinsic difference in fractionation behavior between bacterial pure cultures
467 and the presumably more complex nitrifier community present in soils at the study site, or is due to
468 our assumption of constant $^{18}\varepsilon_{comp}$ and $^{18}\varepsilon_{k,H2O,2}$ between fertilized and non-fertilized treatments
469 required to solve for these two terms. Regardless, the positive identification of $^{18}\varepsilon_{comp}$ and $^{18}\varepsilon_{k,H2O,2}$ is
470 in line with the consensus reached in pure culture studies that enzyme-mediated extractions of O
471 atoms from water and O_2 and subsequent incorporations into nitrification-produced NO_3^- are
472 associated with large kinetic fractionations.

473 Based on the current understanding of the fractionation mechanisms underlying $\delta^{18}O_{NO3,nit}$,
474 Boshers et al. (2019) conducted a numerical simulation to show that $\delta^{18}O_{NO3,nit}$ can be largely
475 constrained to be within ±3‰ of the corresponding $\delta^{18}O_{H2O}$. In our case, when using the NO_3^- load-
476 weighted mean $\delta^{18}O_{H2O}$ of tile drainage (-6.3‰), $\delta^{18}O_{NO3,nit}$ was predicted to range between -5.8‰ and
477 -1.9‰. Therefore, our results support the conclusion of Boshers et al. (2019) and advocate a
478 homologous model of $\delta^{18}O_{NO3,nit}$ for both nitrifying pure cultures and soil systems. These results also
479 challenge the simplifying assumption adopted by many recent watershed studies that $\delta^{18}O_{NO3,nit}$ is
480 solely dependent on the $\delta^{18}O$ values of O_2 and water and the proportional contribution of these two O

sources during nitrification. More studies are needed to quantify $\delta^{18}O_{NO3,nit}$ in soils from a broad range of environments and to more completely understand the variability of $\delta^{18}O_{NO3,nit}$ under varying thermodynamic and kinetic conditions.

4.2. Source and transport mechanisms for tile drainage NO_3^- export.

The tile drainage measurements revealed marked chemostasis in NO_3^- export across all three cropping phases at our study site (Fig. 5 left column). The observation that variation in tile NO_3^- loads was predominantly determined by changes in tile discharge rather than NO_3^- concentration indicates transport-limited systems and the likely presence of a large NO_3^- store that can be readily mobilized in proportion to flow generation (Basu et al., 2010; Thompson et al., 2011). This interpretation is conceptually supported by the isotopic composition of NO_3^- in tile drainage measured during the corn non-growing season and soybean year. Specifically, variations in $\delta^{15}N_{NO3}$ and $\delta^{18}O_{NO3}$ observed during these periods were strongly coupled (Fig. 6). Moreover, among all potential NO_3^- sinks measured (i.e., soil TN and crop biomass), only soybean biomass had $\delta^{15}N$ values lower than the temporally integrated $\delta^{15}N$ values of tile drainage NO_3^- (Fig. 7), which can be well explained by biological N_2 fixation carried out by the soybean plants. These observations point to denitrification, rather than NO_3^- assimilation by soil microbes or crop NO_3^- uptake, as the dominant process regulating the coupling and enrichment of $\delta^{15}N_{NO3}$ and $\delta^{18}O_{NO3}$ in tile drainage. Consequently, the observed strong coupling of $\delta^{15}N_{NO3}$ and $\delta^{18}O_{NO3}$ during unfertilized periods implies that tile drainage NO_3^- had an approximately constant $\delta^{15}N_{source}$ value after accounting for denitrification enrichment and was not the product of dynamic mixing of multiple NO_3^- sources with distinct isotopic composition. These results support our assertion that the presence of a large and well-mixed NO_3^- store will result in a temporally invariant source signature of NO_3^- in tile drainage.

The estimated tile drainage $\delta^{15}N_{source}$ values for the corn growing season and soybean year ranged between -4.4‰ and 1.4‰ across the three study tiles (Table 1). These values were similar to the $\delta^{15}N$ values of applied fertilizer NH_3 and soybean biomass but markedly different than soil TN and corn biomass N values (Fig. 7). This comparison implies the potential role of fertilizer- and/or soybean residue-derived N as a persistent source of tile drainage NO_3^- loss, even during the soybean

508 year, when no N fertilizer or soybean residue was input to the soil. In contrast, the $\delta^{15}N_{source}$ values
509 estimated for the corn growing season (-8.3 to -3.0‰) were lower than the $\delta^{15}N$ of all potential N
510 sources in our system (Fig. 7), which is consistent with the characteristically low $\delta^{15}N_{NO3}$ values
511 observed following fertilizer applications (Fig. 4c) and can only be explained by the kinetic N isotope
512 effect resulting from partial nitrification of applied fertilizer NH_3 (Fig. 2b).

513 To test the sensitivity of the estimated $\delta^{15}N_{source}$ values to water sources used during
514 nitrification, we explored the possibility that soil nitrification mainly occurred in the aerobic surface
515 soil so that the $\delta^{18}O$ of water used in in-situ nitrification was subject to seasonal variations with the
516 $\delta^{18}O_{H2O}$ of precipitation. We show in Table S3 that $\delta^{15}N_{source}$ values remain essentially unchanged
517 when using temporally integrated precipitation $\delta^{18}O_{H2O}$ values based on the three cropping phases
518 (i.e., -7.3 to -5.1‰) to predict $\delta^{18}O_{NO3,nit}$. This confirms that the use of tile drainage $\delta^{18}O_{H2O}$ values is
519 robust. Additionally, the estimated $\delta^{15}N_{source}$ values are conditioned on the assumption that
520 denitrification exerts an identical fractionation on the N and O isotopes of NO_3^-, such that the slope of
521 denitrification trajectory in dual isotope space is equal to one. This assumption is supported by the
522 approximately 1:1 coupling of $\delta^{15}N_{NO3}$ and $\delta^{18}O_{NO3}$ observed during the corn non-growing season and
523 soybean year (Fig. 6). It is also consistent with the intrinsic N and O isotopic fractionations catalyzed
524 by the *Nar* dissimilatory NO_3^- reductase (Granger et al., 2008; Boettger et al., 2022), which is
525 considered the dominant respiratory pathway for heterotrophic NO_3^- consumption in freshwater
526 systems (Granger and Wankel, 2016). Interestingly, if we include NO_3^- isotope data measured during
527 the corn growing season in the linear regression of $\delta^{15}N_{NO3}$-versus-$\delta^{18}O_{NO3}$, the regression slope is
528 lowered to be around 0.6 (Fig. 6; Table S2). As the $\delta^{15}N_{NO3}$ values measured following fertilizer
529 applications were affected by the kinetic isotope effect for nitrification, this change in the regression
530 slope provides direct evidence for the isotopic overprinting of nitrification on denitrification (Granger
531 and Wankel, 2016). Extending this finding to surface- and groundwater systems, the commonly
532 observed denitrification slopes being lower than one in these systems may partially result from
533 temporal and spatial aggregations of NO_3^- variably fractionated during nitrification and denitrification.

Therefore, the estimated $\delta^{15}N_{source}$ values across all cropping phases depict a bimodal pattern in NO_3^- source production, with fertilizer applications triggering a pulsed release of NO_3^- that shifts $\delta^{15}N_{source}$ in tile drainage from an isotopically uniform pool reflecting NH_3 fertilizer and/or soybean residue N to one that reflects partial nitrification of recently applied NH_3 (Fig. 7; Table 1). This revealed variation in $\delta^{15}N_{source}$ prompts two related questions: (1) how does the soil-plant system store, transport, and partition fertilizer- and/or soybean-derived N, making this N a potentially persistent source of tile drainage NO_3^- loss during unfertilized periods?; and (2) why is there a lack of isotopic signals of the bulk soil N pool and corn biomass in tile drainage NO_3^-?

In our study system, if we assume a fertilizer use efficiency of 40%, which is at the upper end of reported range for cereal cropping (Yan et al., 2020), the amount of fertilizer N not recovered by the same-season corn was about 120 kg N ha^{-1} yr^{-1}. Likewise, the amount of N input via incorporation of aboveground, non-grain soybean biomass was also on the order of 120 kg N ha^{-1} yr^{-1}. Although a large fraction of this N input may be immobilized by soil microbes, the revealed pattern in $\delta^{15}N_{source}$ dynamics seems to suggest a selective mechanism that preferentially stabilizes corn biomass N but renders fertilizer- and/or soybean residue-derived N a labile source for NO_3^- production and loss. This selective mechanism may be driven by stoichiometric imbalances and variable microbial N use efficiency at the soil microsite scale (Schimel and Bennett, 2004; Manzoni et al., 2008). For example, the higher C-to-N ratio of corn residues may create soil microsites with limited N availability, which may subsequently increase microbial N use efficiency and promote tighter recycling of microbial residues (Kaiser et al., 2014; Mooshammer et al., 2014; Zhang et al., 2019). This tightened recycling, combined with the slower decomposition of corn residues compared to soybean residues, may favor the stabilization and sequestration of soluble organic compounds in these N-poor microsites due to greater opportunities for protection through sorption toward mineral surfaces and incorporation into aggregates (Lehmann and Kleber, 2015; Cotrufo et al., 2015). On the other hand, in N-rich soil microsites, such as those receiving direct fertilizer input and/or soybean residues, high N availability may initially stimulate N immobilization and microbial growth (Mooshammer et al., 2014; Zhang et al., 2019). However, as this growth continues, microbial biomass may be increasingly carbon-limited,

561 which may eventually result in elevated microbial mortality, reduced microbial N use efficiency, and
562 recycling of carbon stored in microbial residues (Cui et al., 2020; Li et al., 2021). The release of
563 soluble organic compounds from this recycling may saturate the protection sinks of these N-rich
564 microsites (Castellano et al., 2015), resulting in leakage of NO_3^- via mineralization and subsequent
565 nitrification.

566 Additionally, the revealed chemostatic NO_3^- export regime and $\delta^{15}N_{source}$ dynamics may also
567 result from the large capacity of the soil profile to store water and NO_3^-. Using chloride as a
568 conservative tracer, a previous study at the same field has revealed a total storage capacity of at least
569 1000 mm for tile flow generation (Yu et al. 2023). Assuming a porosity of 0.4 for a silt loam Mollisol,
570 this storage would require a soil depth of at least 2.5 m, which corresponds to the entire above-tile
571 profile plus an additional 1 m of soil below the tile drain. This extensive storage capacity may provide
572 a significant mixing volume for NO_3^- that retains memories of past N input to the soil-plant system
573 (Woo and Kumar, 2019; Williams et al., 2021). Importantly, the presence of this large mixing volume
574 is consistent with the highly dampened variation in the $\delta^{18}O_{H2O}$ values of tile drainage compared to
575 those of precipitation (Fig. 4e). However, on the other hand, a large storage and mixing volume of
576 NO_3^- appears to be at odds with the high sensitivity of tile drainage $\delta^{15}N_{NO3}$ and $\delta^{18}O_{NO3}$ to high flow
577 events (Fig. 5 middle and right columns) and with the direct response of $\delta^{15}N_{NO3}$ to fertilizer
578 applications (Fig, 2c). One way to reconcile these seemingly paradoxical observations is the
579 progressive activation of preferential flows as the soil becomes wetter (Klaus et al., 2013; Williams et
580 al., 2016; Yu et al., 2023). In fine-textured soils with high root density, preferential flows may be
581 facilitated by an extensive network of soil macropores associated with root channels, earthworm
582 burrows, and desiccation cracks (Klaus et al., 2013; Williams et al., 2016). As NO_3^- in the upper
583 depths of the soil profile may have lower $\delta^{15}N_{NO3}$ and $\delta^{18}O_{NO3}$ values due to surface inputs and higher
584 mineralization and nitrification rates relative to denitrification, accelerated transport of water and
585 NO_3^- from these near-surface layers via activated preferential flowpaths under wet conditions can
586 explain the negative relationships between tile discharge and NO_3^- isotopes (Fig. 5 middle and right
587 columns) and the flashy responses of tile drainage water and NO_3^- isotopes observed at the event scale

588 (Fig. 4c, 4d, and 4e) (Yu et al., 2023). Although NO_3^- concentration may also be higher at surface soil
589 depths, the effect of this preferential transport was not readily detected by NO_3^- concentration
590 measurements due to the simultaneous dilution of NO_3^- under high flow conditions.

591 We speculate that the combination of these proposed mechanisms based on soil-microbe
592 interactions at the soil microsite scale and the storage and preferential transport of NO_3^- in the soil
593 profile may account for the variability of $\delta^{15}N_{source}$ in tile drainage. Although we are not able to verify
594 these mechanisms and tease apart their relative importance due to the lack of appropriate data, the
595 observed temporal variations in NO_3^- isotopes provide hints at the emergent modes of NO_3^- source and
596 transport dynamics across the cropping phases. For example, the coupled increase in tile drainage
597 NO_3^- concentrations and the decrease in $\delta^{15}N_{NO3}$ values observed during the corn non-growing season
598 in 2021 and 2023 (Fig. 4b and 4c), combined with the large input of soybean residues during this
599 period, may indicate that mineralization and recycling of soybean residue N were an important
600 contributor of NO_3^- loss during this period. On the other hand, the similarity in $\delta^{15}N_{NO3}$ and $\delta^{18}O_{NO3}$
601 values observed during the soybean year to those measured at the end of the corn growing season in
602 2021 (Fig. 4b and 4c) may imply a delayed release of fertilizer-derived NO_3^- due to water storage and
603 the early cessation of tile flows in the 2021 corn growing season.

604 To reduce NO_3^- loss from tile-drained midwestern agroecosystems, fertilizer management that
605 aims to synchronize N input and crop N demand has been an organizing principle for improving N use
606 efficiency in these systems. However, a recent synthesis based on 1000 site-years of tile drainage
607 NO_3^- loads revealed no significant differences between different fertilizer timing and application
608 methods in reducing tile NO_3^- loss (Christianson and Harmel, 2015). Based on the results of this
609 study, we show that NO_3^- export in tile drainage may be modulated by a N legacy effect that can mask
610 short-term responses – and thus evaluation – of tile drainage NO_3^- loads to changes in management
611 practices. However, we note that the term "legacy effect" should not be taken literally, as any NO_3^-
612 contained in a water sample reflects a mixture of N with different origins and introduced to the system
613 at different times. The legacy effect is a question of degree, and there is evidence that extensive
614 system modifications (e.g., conversion from corn/soybean to perennial biofuel crops) can significantly

615 tighten the N cycle in tile-drained agroecosystems over a short time span (Smith et al., 2013).
616 Nevertheless, the existence of these legacy effects calls for long-term and well controlled field studies,
617 which remain an exception rather than the norm in tile drainage research (Christianson and Harmel,
618 2015; Gentry et al., 2023). It also reinforces the importance of coupling N and carbon cycles in
619 conventionally managed row crop systems via diversification of N source input and plant types in
620 reducing tile drainage NO_3^- loss (Drinkwater and Snapp, 2007).

621 **5. Conclusions**

622 In this study, multiyear measurements of tile drainage NO_3^- isotopes were used to examine the sources
623 and processes controlling NO_3^- export from a tile-drained con-soybean field. These field isotope data
624 were supplemented by characterization of the N isotopic composition of potential NO_3^- sources (i.e.,
625 fertilizer, soil nitrogen, and crop biomass) in the field and by the oxygen isotopic composition of NO_3^-
626 produced by nitrification in soil incubations. To our knowledge, this study represents the first attempt
627 to adopt such a fine-grained approach based on NO_3^- isotopes to examine NO_3^- source and transport
628 mechanisms in terrestrial settings. The results from the soil incubation demonstrated that the $\delta^{18}O$ of
629 NO_3^- produced by soil nitrification ($\delta^{18}O_{NO3,nit}$) is determined by isotopic O exchange between NO_2^-
630 and water and by kinetic isotope effects during O atom incorporation from O_2 and water, consistent
631 with previous studies using nitrifying pure cultures. However, $\delta^{18}O_{NO3,nit}$ was significantly different
632 between fertilized and non-fertilized treatments, indicating that the variability of $\delta^{18}O_{NO3,nit}$ is
633 controlled by nitrification rate through its control on NO_2^- accumulation and, consequently, the
634 potential of NO_2^--water exchange during the nitrification process.

635 While NO_3^- export in tile drainage was characterized by prominent chemostasis, NO_3^-
636 isotopes in tile drainage were highly sensitive to variations in tile discharge and fertilizer input.
637 Following fertilizer applications, the dramatic decline in tile drainage $\delta^{15}N_{NO3}$ values indicates rapid
638 nitrification of applied NH_3 fertilizer and the subsequent loss of the nitrified NO_3^- possibly via
639 preferential flows. On the other hand, variations in tile drainage $\delta^{15}N_{NO3}$ and $\delta^{18}O_{NO3}$ values were
640 strongly coupled during unfertilized periods (i.e., corn non-growing season and soybean year),
641 suggesting denitrification as a dominant process regulating the temporal variation of NO_3^- isotopes

during these periods. Moreover, this strong coupling provides evidence for an approximately constant NO_3^- isotopic source signature, as opposed to a dynamic mixing of multiple NO_3^- sources with distinct isotopic signatures. Combining the field NO_3^- and water isotope measurements with the O isotopic systematics of soil nitrification revealed a dynamic NO_3^- source mechanism, with fertilizer applications triggering a pulsed release of NO_3^- that shifts the isotopic signature of NO_3^- from an isotopically uniform pool reflecting NH_3 fertilizer and/or soybean residue N to one that reflects partial nitrification of recently applied NH_3. These results imply that fertilizer- and/or soybean residue-derived N was a persistent source of tile drainage NO_3^- export during unfertilized periods and highlights a N legacy effect possibly resulting from N recycling at the soil microsite scale and a large storage and mixing capacity of NO_3^- in the soil. While more research is needed to examine the coupled biogeochemical and hydrological processes regulating the formation of legacy N stores and their impact on NO_3^- export in tile-drained agroecosystems, through this study, we demonstrated the unique strength of NO_3^- isotopes as an integrative tracer for probing complex N source and transport mechanisms under heterogeneous field conditions and how a rigorous understanding of isotopic fractionations (e.g., those underlying $\delta^{18}O_{NO3,nit}$) is key to maximizing this strength.

Acknowledgements

This work was funded by USDA-NIFA Hatch Project ILLU-875-983 and the Illinois Nutrient Research and Education Council (Project 2021-4-360649-46 and 2014-5-360847-320). We are grateful to John Green for the collection of tile drainage samples. We also thank Naglis Subacius and Nora Danaher for their assistance with laboratory analyses.

Data Availability Statement

The data that support the findings of this study, including those collected during the laboratory incubation and field tile drainage measurements, are available at Hu and Yu (2024).

References

Andersson, K.K. and Hooper, A.B., 1983. O_2 and H_2O are each the source of one O in NO_2^- produced from NH_3 by Nitrosomonas: ^{15}N-NMR evidence. *Febs Letters*, *164*(2), pp.236-240.

Andersson, K.K., Philson, S.B. and Hooper, A.B., 1982. ^{18}O isotope shift in ^{15}N NMR analysis of biological N-oxidations: H_2O-NO_2^- exchange in the ammonia-oxidizing bacterium Nitrosomonas. *Proceedings of the National Academy of Sciences*, *79*(19), pp.5871-5875.

Basu, N.B., Destouni, G., Jawitz, J.W., Thompson, S.E., Loukinova, N.V., Darracq, A., Zanardo, S., Yaeger, M., Sivapalan, M., Rinaldo, A. and Rao, P.S.C., 2010. Nutrient loads exported from managed catchments reveal emergent biogeochemical stationarity. *Geophysical Research Letters*, *37*(23).

Bauwe, A., Kahle, P., Tiemeyer, B. and Lennartz, B., 2020. Hydrology is the key factor for nitrogen export from tile-drained catchments under consistent land-management. *Environmental Research Letters*, *15*(9), p.094050.

Blann, K.L., Anderson, J.L., Sands, G.R. and Vondracek, B., 2009. Effects of agricultural drainage on aquatic ecosystems: a review. *Critical reviews in environmental science and technology*, *39*(11), pp.909-1001.

Boettger, J.D., Neubauer, C., Kopf, S.H. and Kubicki, J.D., 2022. Microbial Denitrification: Active Site and Reaction Path Models Predict New Isotopic Fingerprints. *ACS Earth and Space Chemistry*, *6*(11), pp.2582-2594.

Boshers, D.S., Granger, J., Tobias, C.R., Böhlke, J.K. and Smith, R.L., 2019. Constraining the oxygen isotopic composition of nitrate produced by nitrification. *Environmental Science & Technology*, *53*(3), pp.1206-1216.

Buchwald, C. and Casciotti, K.L., 2010. Oxygen isotopic fractionation and exchange during bacterial nitrite oxidation. *Limnology and Oceanography*, *55*(3), pp.1064-1074.

Buchwald, C. and Casciotti, K.L., 2013. Isotopic ratios of nitrite as tracers of the sources and age of oceanic nitrite. *Nature Geoscience*, *6*(4), pp.308-313.

Buchwald, C., Santoro, A.E., McIlvin, M.R. and Casciotti, K.L., 2012. Oxygen isotopic composition of nitrate and nitrite produced by nitrifying cocultures and natural marine assemblages. *Limnology and Oceanography*, *57*(5), pp.1361-1375.

Casciotti, K.L., Böhlke, J.K., McIlvin, M.R., Mroczkowski, S.J. and Hannon, J.E., 2007. Oxygen isotopes in nitrite: Analysis, calibration, and equilibration. *Analytical Chemistry*, *79*(6), pp.2427-2436.

Casciotti, K.L., McIlvin, M. and Buchwald, C., 2010. Oxygen isotopic exchange and fractionation during bacterial ammonia oxidation. *Limnology and Oceanography*, *55*(2), pp.753-762.

Casciotti, K.L., Sigman, D.M. and Ward, B.B., 2003. Linking diversity and stable isotope fractionation in ammonia-oxidizing bacteria. *Geomicrobiology Journal*, *20*(4), pp.335-353.

Castellano, M.J., Archontoulis, S.V., Helmers, M.J., Poffenbarger, H.J. and Six, J., 2019. Sustainable intensification of agricultural drainage. *Nature Sustainability*, *2*(10), pp.914-921.

Castellano, M.J., Mueller, K.E., Olk, D.C., Sawyer, J.E. and Six, J., 2015. Integrating plant litter quality, soil organic matter stabilization, and the carbon saturation concept. *Global Change Biology*, *21*(9), pp.3200-3209.

Christianson, L.E. and Harmel, R.D., 2015. 4R Water quality impacts: An assessment and synthesis of forty years of drainage nitrogen losses. *Journal of Environmental Quality*, *44*(6), pp.1852-1860.

Cotrufo, M.F., Soong, J.L., Horton, A.J., Campbell, E.E., Haddix, M.L., Wall, D.H. and Parton, W.J., 2015. Formation of soil organic matter via biochemical and physical pathways of litter mass loss. *Nature Geoscience*, *8*(10), pp.776-779.

Cui, J., Zhu, Z., Xu, X., Liu, S., Jones, D.L., Kuzyakov, Y., Shibistova, O., Wu, J. and Ge, T., 2020. Carbon and nitrogen recycling from microbial necromass to cope with C: N stoichiometric imbalance by priming. *Soil Biology and Biochemistry*, *142*, p.107720.

Danalatos, G.J., Wolter, C., Archontoulis, S.V. and Castellano, M.J., 2022. *Nitrate losses across 29 Iowa watersheds: Measuring long-term trends in the context of interannual variability* (Vol. 51, No. 4, pp. 708-718).

David, M.B., Drinkwater, L.E. and McIsaac, G.F., 2010. Sources of nitrate yields in the Mississippi River Basin. *Journal of environmental quality*, *39*(5), pp.1657-1667.

Drinkwater, L.E. and Snapp, S., 2007. Nutrients in agroecosystems: rethinking the management paradigm. *Advances in Agronomy*, *92*, pp.163-186.

Gardner, J.B. and Drinkwater, L.E., 2009. The fate of nitrogen in grain cropping systems: a meta-analysis of ^{15}N field experiments. *Ecological applications*, *19*(8), pp.2167-2184.

Gentry, L.E., Green, J.M., Mitchell, C.A., Andino, L.F., Rolf, M.K., Schaefer, D. and Nafziger, E.D., 2023. Split fertilizer nitrogen application with a cereal rye cover crop reduces tile nitrate loads in a corn-soybean rotation. *Journal of Environmental Quality*.

Giguere, A.T., Taylor, A.E., Myrold, D.D., Mellbye, B.L., Sayavedra-Soto, L.A. and Bottomley, P.J., 2018. Nitrite-oxidizing activity responds to nitrite accumulation in soil. *FEMS microbiology ecology*, *94*(3), p.fiy008.

Godsey, S.E., Kirchner, J.W. and Clow, D.W., 2009. Concentration–discharge relationships reflect chemostatic characteristics of US catchments. *Hydrological Processes*, *23*(13), pp.1844-1864.

Granger, J. and Sigman, D.M., 2009. Removal of nitrite with sulfamic acid for nitrate N and O isotope analysis with the denitrifier method. *Rapid Communications in Mass Spectrometry*, *23*(23), pp.3753-3762.

Granger, J. and Wankel, S.D., 2016. Isotopic overprinting of nitrification on denitrification as a ubiquitous and unifying feature of environmental nitrogen cycling. *Proceedings of the National Academy of Sciences*, *113*(42), pp.E6391-E6400.

Granger, J., Sigman, D.M., Lehmann, M.F. and Tortell, P.D., 2008. Nitrogen and oxygen isotope fractionation during dissimilatory nitrate reduction by denitrifying bacteria. *Limnology and Oceanography*, *53*(6), pp.2533-2545.

Gruber, N. and Galloway, J.N., 2008. An Earth-system perspective of the global nitrogen cycle. *Nature*, *451*(7176), pp.293-296.

Hu, Y. and Yu, Z., 2024. Deciphering the isotopic imprint of nitrate to reveal nitrogen source and transport mechanisms in a tile-drained agroecosystem [Dataset]. Zenodo. https://doi.org/10.5281/zenodo.10515753

Jones, R.W. and Hedlin, R.A., 1970. Ammonium, nitrite and nitrate accumulation in three Manitoba soils as influenced by added ammonium sulfate and urea. *Canadian Journal of Soil Science*, *50*(3), pp.331-338.

Kaiser, C., Franklin, O., Dieckmann, U. and Richter, A., 2014. Microbial community dynamics alleviate stoichiometric constraints during litter decay. *Ecology letters*, *17*(6), pp.680-690.

Kendall, C., Elliott, E.M. and Wankel, S.D., 2007. Tracing anthropogenic inputs of nitrogen to ecosystems. *Stable isotopes in ecology and environmental science*, pp.375-449.

Klaus, J., Zehe, E., Elsner, M., Külls, C. and McDonnell, J.J., 2013. Macropore flow of old water revisited: experimental insights from a tile-drained hillslope. *Hydrology and Earth System Sciences*, *17*(1), pp.103-118.

Kroopnick, P. and Craig, H., 1972. Atmospheric oxygen: isotopic composition and solubility fractionation. *Science*, *175*(4017), pp.54-55.

Kumar, S., Nicholas, D.J.D. and Williams, E.H., 1983. Definitive ^{15}N NMR evidence that water serves as a source of 'O'during nitrite oxidation by Nitrobacter agilis. *FEBS letters*, *152*(1), pp.71-74.

Lehmann, J. and Kleber, M., 2015. The contentious nature of soil organic matter. *Nature*, *528*(7580), pp.60-68.

Li, J., Sang, C., Yang, J., Qu, L., Xia, Z., Sun, H., Jiang, P., Wang, X., He, H. and Wang, C., 2021. Stoichiometric imbalance and microbial community regulate microbial elements use efficiencies under nitrogen addition. *Soil Biology and Biochemistry*, *156*, p.108207.

Maharjan, B. and Venterea, R.T., 2013. Nitrite intensity explains N management effects on N_2O emissions in maize. *Soil Biology and Biochemistry*, *66*, pp.229-238.

Manzoni, S., Porporato, A. and Schimel, J.P., 2008. Soil heterogeneity in lumped mineralization–immobilization models. *Soil Biology and Biochemistry*, *40*(5), pp.1137-1148.

Mariotti, A., Germon, J.C., Hubert, P., Kaiser, P., Letolle, R., Tardieux, A. and Tardieux, P., 1981. Experimental determination of nitrogen kinetic isotope fractionation: some principles; illustration for the denitrification and nitrification processes. *Plant and soil*, *62*, pp.413-430.

Mooshammer, M., Wanek, W., Hämmerle, I., Fuchslueger, L., Hofhansl, F., Knoltsch, A., Schnecker, J., Takriti, M., Watzka, M., Wild, B. and Keiblinger, K.M., 2014. Adjustment of microbial nitrogen use efficiency to carbon: nitrogen imbalances regulates soil nitrogen cycling. *Nature Communications*, *5*(1), p.3694.

NADP. (2023). National atmospheric deposition program for Bonville, Illinois (site ID IL11). Retrieved from https://www.usgs.gov/mission-areas/water-resources/science/national-atmospheric-deposition-program-nadp

Nishizawa, M., Sakai, S., Konno, U., Nakahara, N., Takaki, Y., Saito, Y., Imachi, H., Tasumi, E., Makabe, A., Koba, K. and Takai, K., 2016. Nitrogen and oxygen isotope effects of ammonia oxidation by thermophilic Thaumarchaeota from a geothermal water stream. *Applied and Environmental Microbiology*, *82*(15), pp.4492-4504.

Schimel, J.P. and Bennett, J., 2004. Nitrogen mineralization: challenges of a changing paradigm. *Ecology*, *85*(3), pp.591-602.

Smith, C.M., David, M.B., Mitchell, C.A., Masters, M.D., Anderson-Teixeira, K.J., Bernacchi, C.J. and DeLucia, E.H., 2013. Reduced nitrogen losses after conversion of row crop agriculture to perennial biofuel crops. *Journal of environmental quality*, *42*(1), pp.219-228.

Smith, R.V., Doyle, R.M., Burns, L.C. and Stevens, R.J., 1997. A model for nitrite accumulation in soils. *Soil Biology and Biochemistry*, *29*(8), pp.1241-1247.

Snider, D.M., Spoelstra, J., Schiff, S.L. and Venkiteswaran, J.J., 2010. Stable oxygen isotope ratios of nitrate produced from nitrification: ^{18}O-labeled water incubations of agricultural and temperate forest soils. *Environmental Science & Technology*, *44*(14), pp.5358-5364.

Taylor, A.E., Myrold, D.D. and Bottomley, P.J., 2019. Temperature affects the kinetics of nitrite oxidation and nitrification coupling in four agricultural soils. *Soil Biology and Biochemistry*, *136*, p.107523.

Thompson, S.E., Basu, N.B., Lascurain Jr, J., Aubeneau, A. and Rao, P.S.C., 2011. Relative dominance of hydrologic versus biogeochemical factors on solute export across impact gradients. *Water Resources Research*, *47*(10).

USDA-NRCS, 2016. Gridded Soil Survey Geographic (gSSURGO) database for Douglas County, 1199 Illinois. Retrieved from https://gdg.sc.egov.usda.gov/

Valayamkunnath, P., Barlage, M., Chen, F., Gochis, D.J. and Franz, K.J., 2020. Mapping of 30-meter resolution tile-drained croplands using a geospatial modeling approach. *Scientific data*, *7*(1), p.257.

Van Meter, K.J., Van Cappellen, P. and Basu, N.B., 2018. Legacy nitrogen may prevent achievement of water quality goals in the Gulf of Mexico. *Science*, *360*(6387), pp.427-430.

Venterea, R.T., 2007. Nitrite-driven nitrous oxide production under aerobic soil conditions: kinetics and biochemical controls. *Global Change Biology*, *13*(8), pp.1798-1809.

Weigand, M.A., Foriel, J., Barnett, B., Oleynik, S. and Sigman, D.M., 2016. Updates to instrumentation and protocols for isotopic analysis of nitrate by the denitrifier method. *Rapid Communications in Mass Spectrometry*, *30*(12), pp.1365-1383.

Williams, M.R. and McAfee, S.J., 2021. Water storage, mixing, and fluxes in tile-drained agricultural fields inferred from stable water isotopes. *Journal of Hydrology*, *599*, p.126347.

Williams, M.R., King, K.W., Ford, W., Buda, A.R. and Kennedy, C.D., 2016. Effect of tillage on macropore flow and phosphorus transport to tile drains. *Water Resources Research*, *52*(4), pp.2868-2882.

Woo, D.K. and Kumar, P., 2019. Impacts of subsurface tile drainage on age—Concentration dynamics of inorganic nitrogen in soil. *Water Resources Research*, *55*(2), pp.1470-1489.

Yan, M., Pan, G., Lavallee, J.M. and Conant, R.T., 2020. Rethinking sources of nitrogen to cereal crops. *Global Change Biology*, *26*(1), pp.191-199.

Yu, Z. and Elliott, E.M., 2018. Probing soil nitrification and nitrate consumption using $\Delta^{17}O$ of soil nitrate. *Soil Biology and Biochemistry*, *127*, pp.187-199.

Yu, Z., Hu, Y., Gentry, L.E., Yang, W.H., Margenot, A.J., Guan, K., Mitchell, C.A. and Hu, M., 2023. Linking water age, nitrate export regime, and nitrate isotope biogeochemistry in a tile-drained agricultural field. *Water Resources Research*, *59*(12), e2023WR034948.

Zhang, S., Zheng, Q., Noll, L., Hu, Y. and Wanek, W., 2019. Environmental effects on soil microbial nitrogen use efficiency are controlled by allocation of organic nitrogen to microbial growth and regulate gross N mineralization. *Soil Biology and Biochemistry*, *135*, pp.304-315.

Table and Figures

Table 1. $\delta^{15}N_{source}$ values in ‰ for the three tiles and three cropping phases estimated based on NO_3^- load-weighted mean $\delta^{18}O_{H2O}$ values of tile drainage.

	Corn growing season		Corn non-growing season		Soybean year	
	$\delta^{18}O_{H2O}$	$\delta^{15}N_{source}$	$\delta^{18}O_{H2O}$	$\delta^{15}N_{source}$	$\delta^{18}O_{H2O}$	$\delta^{15}N_{source}$
Tile A	-6.1	-7.1 to -3.0	-6.5	-3.1 to 0.8	-6.2	-2.6 to 1.4
Tile B	-5.9	-8.3 to -4.2	-6.4	-4.4 to -0.4	-6.2	-4.7 to -0.7
Tile C	-6.1	-8.0 to -4.0	-5.9	-3.8 to 0.3	-6.5	-4.8 to -0.9

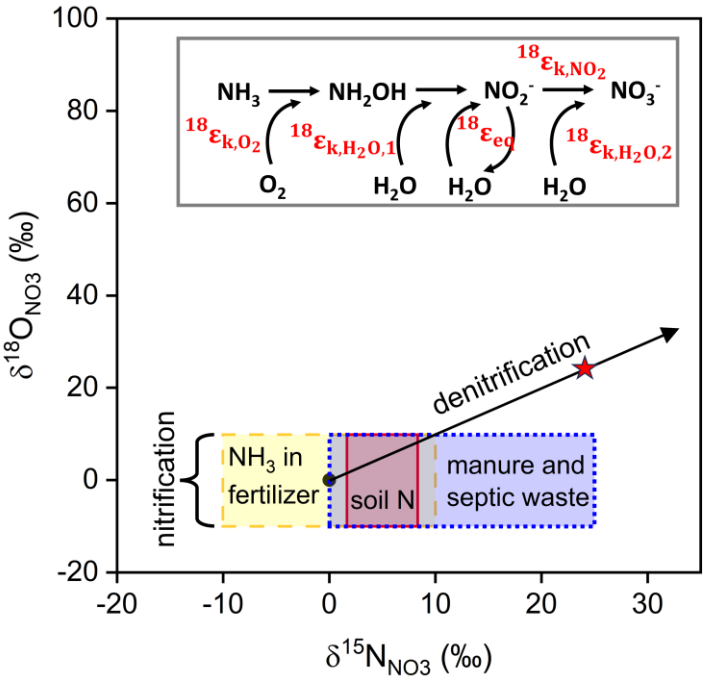

834

835 **Figure 1**. Dual NO_3^- isotope space adapted from Kendall et al. (2007). Shaded boxes indicate typical
836 $\delta^{15}N$ and $\delta^{18}O$ values of NO_3^- derived or nitrified from various N sources. The typically assumed
837 range of $\delta^{18}O_{NO3}$ values produced from nitrification of NH_3 and organic N (-10 to 10‰) are denoted
838 by "nitrification". The black arrow indicates the linear denitrification trajectory that reflects the
839 coupled N and O isotopic fractionations during denitrification. Along this arrow, the filled cycle
840 represents the initial isotopic composition (i.e., source signature) of NO_3^-, while the red star indicates
841 NO_3^- isotopic composition after denitrification enrichment. A schematic diagram of O isotopic
842 fractionations and exchange during nitrification is shown in the insert. Sources of O atoms (O_2 and
843 water) for NH_3 and NO_2^- oxidation are shown, as well as O isotope effects associated with O atom
844 incorporation ($^{18}\varepsilon_{k,O2}$, $^{18}\varepsilon_{k,H2O,1}$, and $^{18}\varepsilon_{k,H2O,2}$), NO_2^--water equilibrium ($^{18}\varepsilon_{eq}$), and NO_2^- oxidation
845 ($^{18}\varepsilon_{k,NO2}$). Detailed descriptions of the O isotope effects are provided in Section 3.4.

846

847

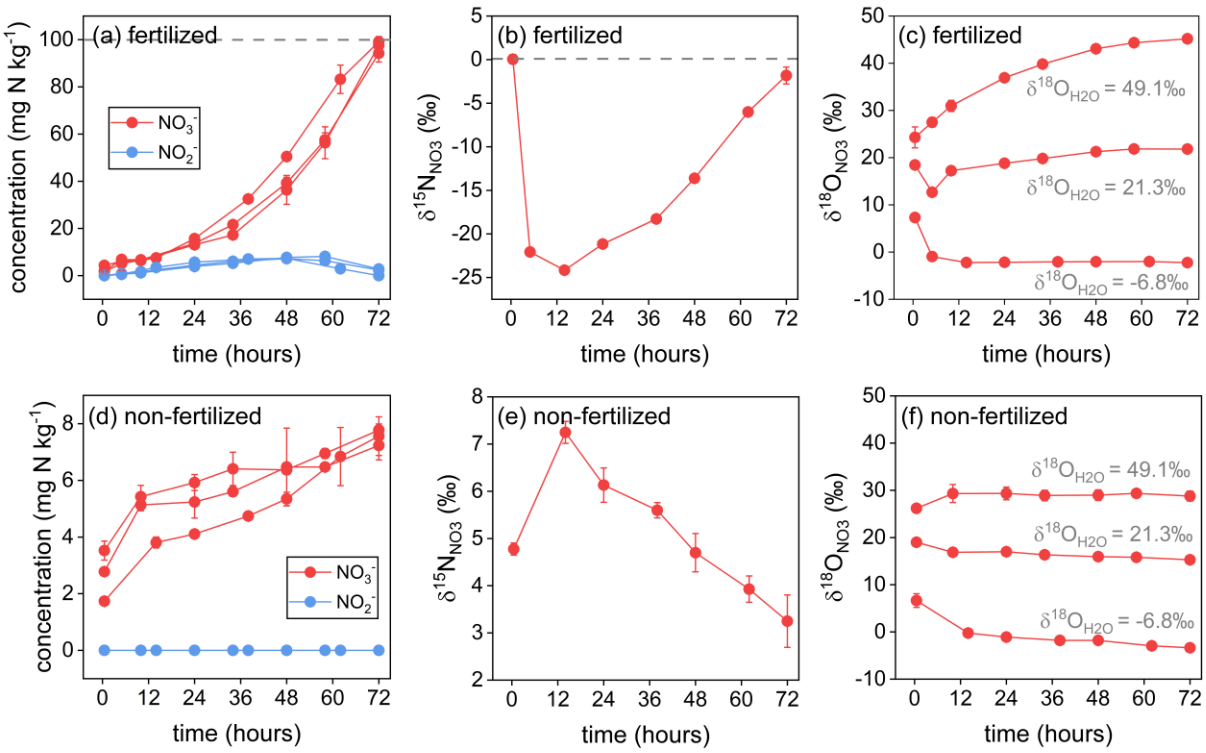

Figure 2. Temporal evolution of soil NO_3^- and NO_2^- concentrations (a and c), $\delta^{15}N_{NO3}$ values (b and e) and $\delta^{18}O_{NO3}$ values (c and f) for the three $\delta^{18}O_{H2O}$ treatments with and without fertilization. Error bars correspond to the standard deviation of replicate measurements. The horizontal dashed line denotes the initial concentration of amended NH_4^+ in (a) and the initial $\delta^{15}N$ of amended NH_4^+ in (b). Text labels in (c) and (f) differentiate measured $\delta^{18}O_{NO3}$ values among the three $\delta^{18}O_{H2O}$ treatments.

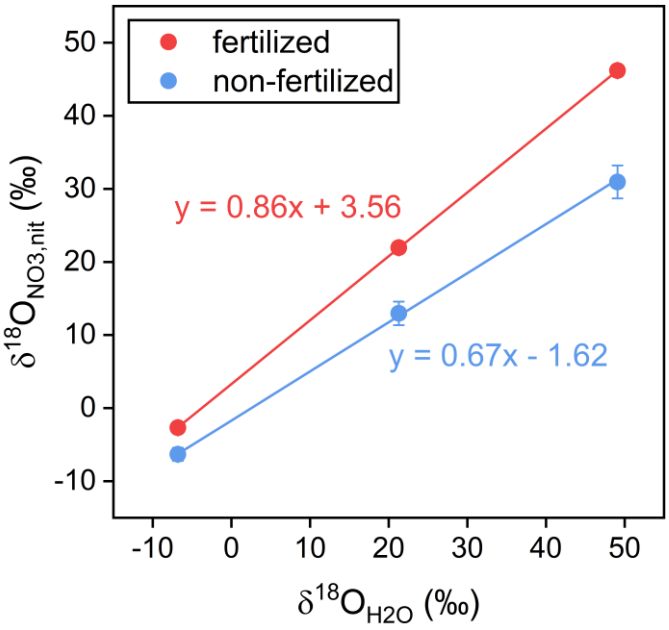

857

858 **Figure 3**. Dependence of $\delta^{18}O_{NO3,nit}$ on $\delta^{18}O_{H2O}$ under the fertilized and non-fertilized conditions.

859 Equations correspond to the linear regression fit of the observations.

860

861

862

863

864

865

866

867

868

869

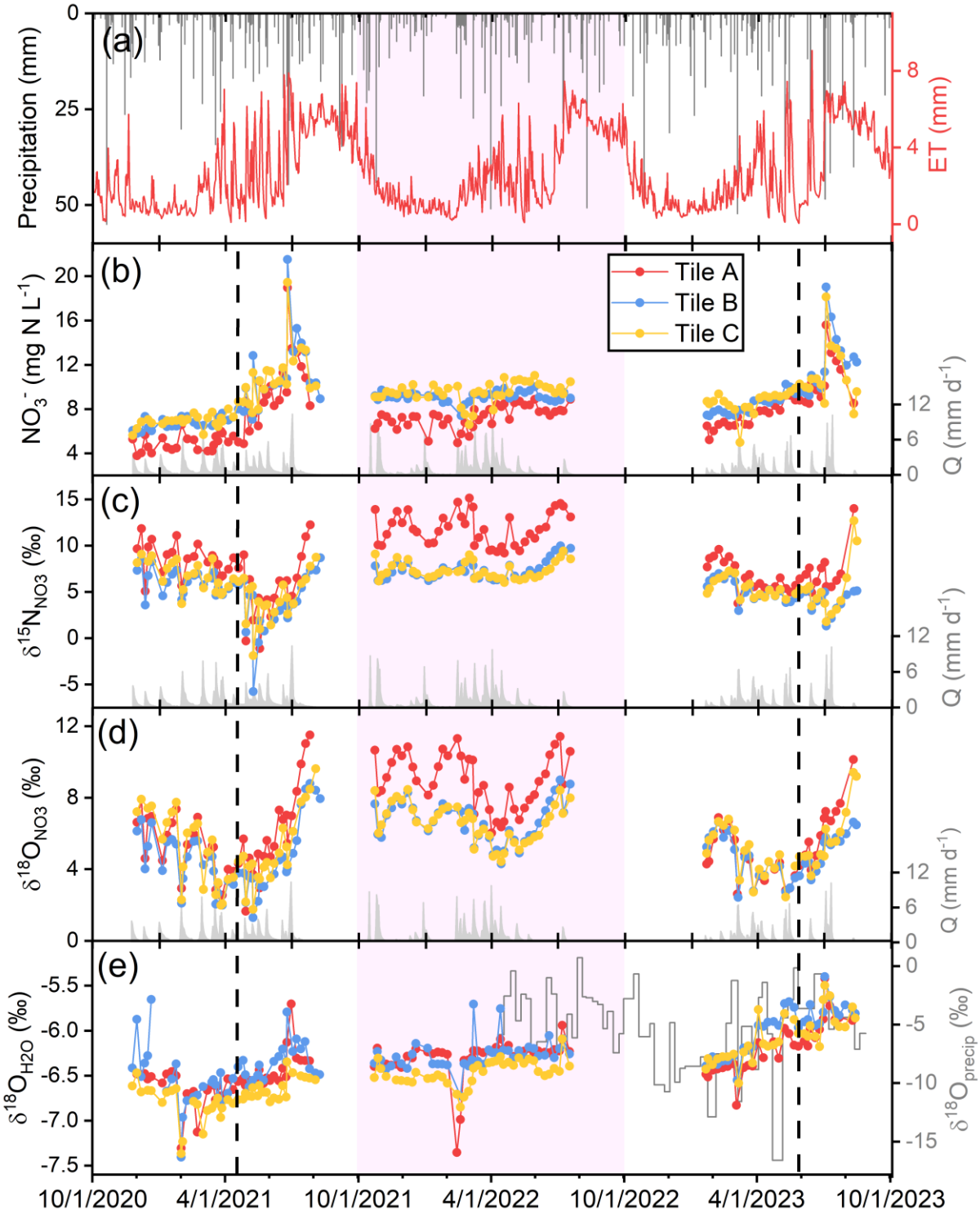

Figure 4. Temporal variations of precipitation and evapotranspiration (ET) (a), NO_3^- concentrations in tile drainage (b), $\delta^{15}N_{NO3}$ values (c), $\delta^{18}O_{NO3}$ values (d), and $\delta^{18}O_{H2O}$ values of tile drainage and weekly cumulative precipitation (e) at the tile-drained field. The black vertical dashed lines indicate the timing of anhydrous NH_3 application in the 2021 and 2023 corn years, respectively. Faded area

denotes the 2022 soybean year. Tile discharge (Q) measured at Tile B is shown in gray in panels b, c, and d to aid interpretation of NO_3^- concentration and isotope data.

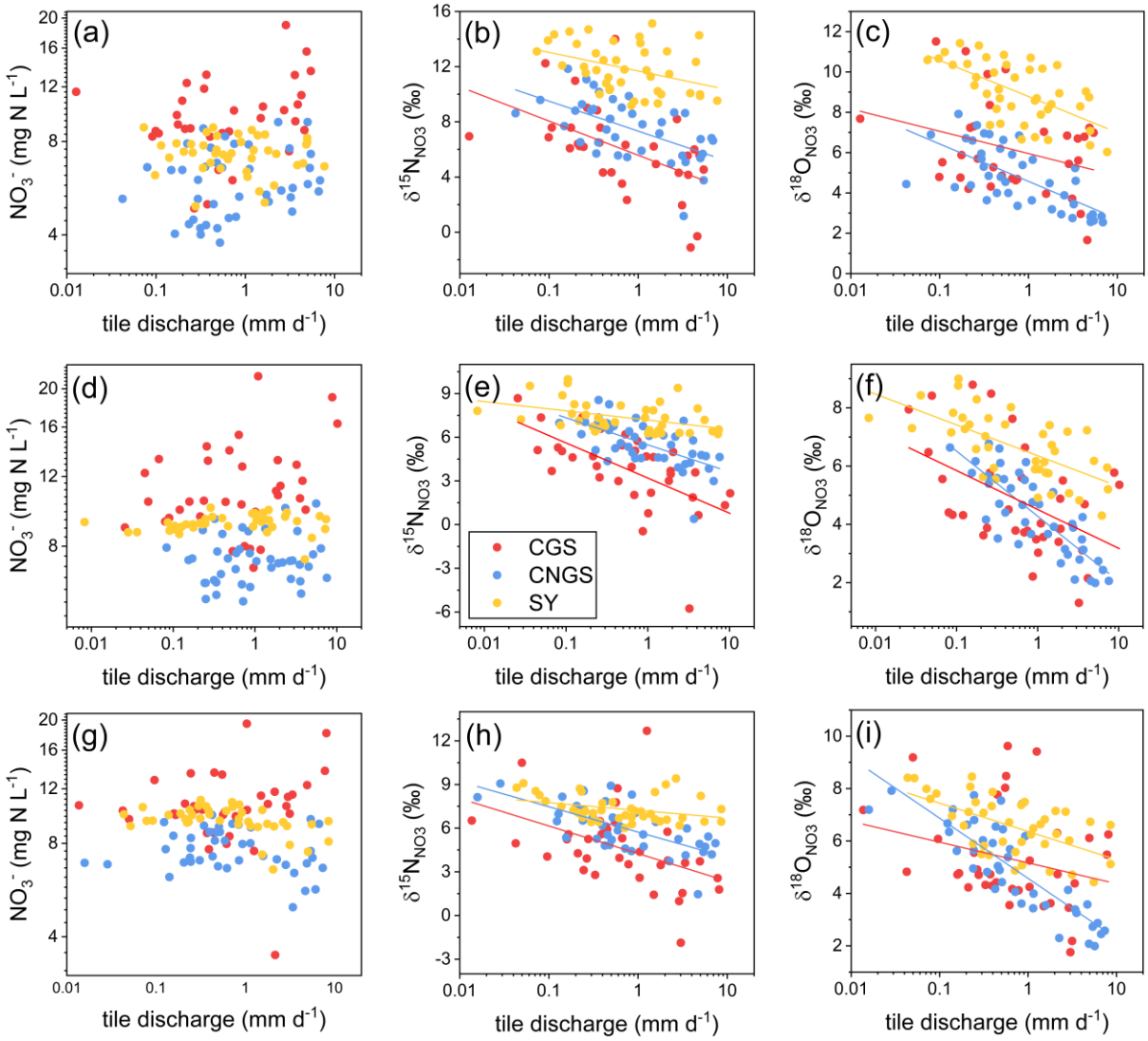

Figure 5. Relationships between tile discharge and NO_3^- concentration (a, d, g; left column), between tile discharge and $\delta^{15}N_{NO3}$ value (b, e, h; middle column), and between tile discharge and $\delta^{18}O_{NO3}$ value (c, f, i; right column), for the three tiles (top row for Tile A, middle row for Tile B, and bottom row for Tile C) and three cropping phases. Note that NO_3^- concentration and tile discharge are shown in logarithmic scale. Linear regression fits for log-transformed tile discharge and NO_3^- isotopes significant at the 0.05 level are also shown. 'CGS', 'CNGS', and 'SY' in the legend denote corn growing season, corn non-growing season, and soybean year, respectively.

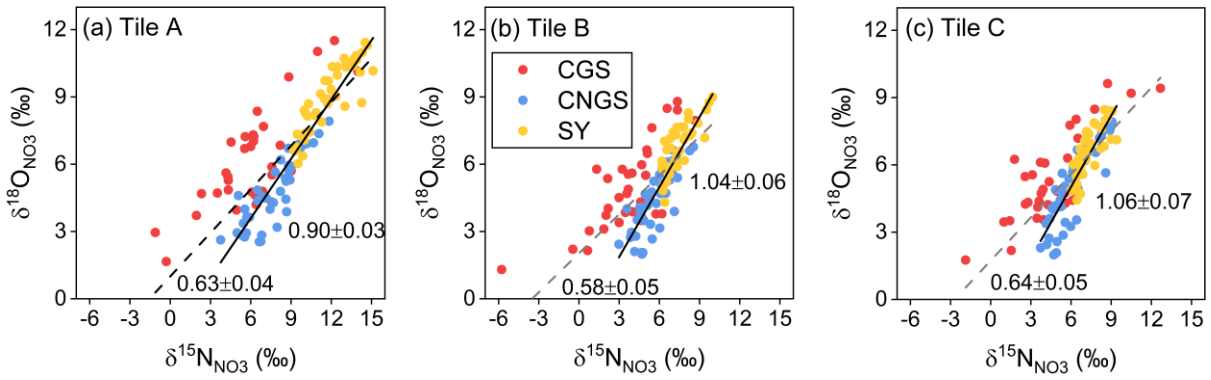

886

887 **Figure 6**. Biplots of $\delta^{15}N_{NO3}$ versus $\delta^{18}O_{NO3}$ values for the three tiles and three cropping phases (a-c).
888 The solid line denotes linear regression based on NO_3^- isotopes measured during the corn non-
889 growing season and soybean season. The dashed line denotes linear regression based on all NO_3^-
890 isotope data. Linear regression slopes (±1 SE) are also shown. 'CGS', 'CNGS', and 'SY' in the legend
891 denote corn growing season, corn non-growing season, and soybean year, respectively.

892

893

894

895

896

897

898

899

900

901

902

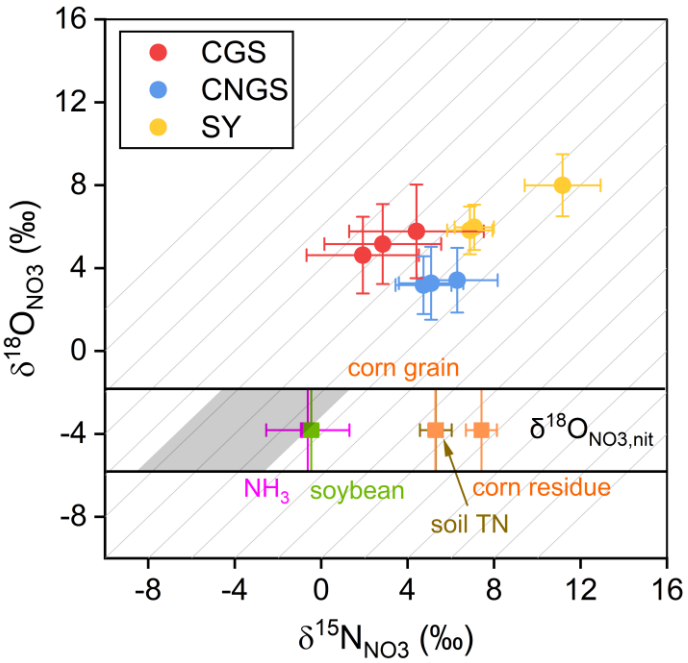

903

904 **Figure 7**. NO_3^- source characterization in dual isotope space. Area encompassed by the solid
905 horizontal lines denotes the predicted range of $\delta^{18}O_{NO3,nit}$ based on the empirical $\delta^{18}O_{NO3,nit}$-versus-
906 $\delta^{18}O_{H2O}$ relationships derived from the soil nitrification experiment. Squares and error bars correspond
907 to the $\delta^{15}N$ and $\delta^{18}O$ values of NO_3^- nitrified from applied NH_3 fertilizer (magenta), soil total N
908 (brown), soybean biomass N (green), and corn biomass N (orange). Dots denote NO_3^- load-weighted
909 mean $\delta^{15}N_{NO3}$ and $\delta^{18}O_{NO3}$ values for the three tiles and three cropping phases. The error bars of the
910 dots reflect the standard deviation of weekly $\delta^{15}N_{NO3}$ and $\delta^{18}O_{NO3}$ values measured during each tile
911 and cropping phase. The grey shaded area corresponds to the range of $\delta^{15}N_{source}$ when considering all
912 tiles and cropping phases collectively. Diagonal grey lines denote denitrification trajectories with a
913 slope of 1. 'CGS', 'CNGS', and 'SY' in the legend denote corn growing season, corn non-growing
914 season, and soybean year, respectively.